Lawrence Berkeley National Laboratory

Title

Assessment of the Second-Ionization Potential of Lawrencium: Investigating the End of the Actinide Series with a One-Atom-at-a-Time Gas-Phase Ion Chemistry Technique

Permalink

Journal

ISSN

Authors

Kwarsick, Jeffrey T
Pore, Jennifer L
Gates, Jacklyn M
et al.

Publication Date

DOI

The Assessment of the Second-Ionization Potential of Lawrencium: Investigating the End of the Actinide Series with a One-Atom-at-a-Time Gas-Phase Ion Chemistry Technique

Jeffrey T. Kwarsick[a,b], Jennifer L. Pore[b,*], Jacklyn M. Gates[b], Kenneth E. Gregorich[b†], John K. Gibson[b], Jiwen Jian[b‡], Gregory K. Pang[b], David K. Shuh[b]

[a]*University of California, Berkeley, Department of Chemistry, Berkeley, CA 94720*
[b]*Lawrence Berkeley National Laboratory, Berkeley, CA 94720*

ABSTRACT:
Experiments were performed at the Lawrence Berkeley National Laboratory 88-Inch Cyclotron facility to investigate the electron-transfer reduction reaction of dipositive Lr (Z = 103) with O_2 gas. Ions of ^{255}Lr were produced in the fusion-evaporation reaction ^{209}Bi(^{48}Ca,2n)^{255}Lr and were studied with a novel gas phase ion chemistry technique. The produced ^{255}Lr^{2+} ions were trapped and O_2 gas was introduced, such that the charge-exchange reaction to reduce ^{255}Lr^{2+} to ^{255}Lr^{1+} was observed and a reaction rate constant was determined to be $k = 1.5(7) \times 10^{-10}$ cm^3/mol/s. The observation that this reaction proceeds, establishes the lower limit on the second ionization potential of Lr to be 13.3(3) eV. This gives further support that the actinide series terminates with Lr. Additionally, this result can be used to better interpret the situation concerning the placement of Lu and Lr on the Periodic Table within the current framework of the Actinide Hypothesis. The success of this experimental approach now identifies unique opportunities for future gas-phase reaction studies on actinide and super heavy elements.

Keywords: actinide elements, transactinide elements, ion-molecule reactions, FIONA mass separator

1. Introduction

There is presently limited information on the fundamental-chemical properties of heavy (Z > 92) and superheavy elements (SHEs, Z >103). It has been predicted that the chemical behavior of these elements may be different from the established periodic trends displayed by their lighter homologues[1]. This is attributed to increased relativistic effects that influence their electronic configurations and significantly affect the nature of their chemical reactivity . Direct-experimental studies to determine fundamental-chemical properties are necessary to understand the magnitude of the relativistic effects, i.e. how much electron orbitals are either contracted or expanded, on the respective heavy element species. The results of direct-experimental studies of these heavy and super heavy elements would be critical benchmarks to aid theoretical predictions [1-5]. Importantly, these measurements would also provide new insight as to the accurate arrangement of the elements in the Periodic Table of the Elements. Even today, proper element placement is still debated. The results of this work show new experimental capabilities that make it possible to perform such measurements.

The structure and organization of the Periodic Table of the Elements is intended to reflect the quantum nature of the atom. It is meant to be a general, easy-to-follow reference road map for the filling of electron orbitals; recognizing and grouping elements that have similar chemical properties; and for navigating other Periodic Trends such as increasing and decreasing atomic

radii. However, despite this intention, several anomalies exist within the current Periodic Table that do not fit the generally agreed-upon rules. Presently, there is much discussion on the accurate placement of the elements Lu (*Z*=71) and Lr (*Z*=103) [6]. The question is whether or not Lu and Lr, should terminate the 4f and 5f blocks, concluding the lanthanide and actinide series, respectively [7]. Or, if Lu and Lr should instead be considered as group 3 elements to initiate the 5d and 6d series, respectively [8]. This proposed arrangement would modify Seaborg's Actinide Hypothesis put forth in the 1940's, which declared that the actinide series should end with element 103, Lr [9,10]. Seaborg had declared that the actinide series was completed with the discovery of Lr in 1961 [11]. To add further confusion to the discussion, it has also been suggested that the f-block series could simply be represented as fifteen-element rows, where the actinides Ac-Lr sit below the lanthanides La-Lu, leaving group 3 to contain just the two elements Sc (*Z*=21) and Y (*Z*=39), even though there are only fourteen f elections [12]. This topic is of such interest, that an IUPAC working group has been formed to decide upon the appropriate constitution of group 3 of the periodic table [13]. This working group has requested input from the scientific community on the atomic and chemical properties of Lu and Lr, which might help to settle the debate. However, due to the complexities of this issue, it is unlikely that this issue will be settled on objective means. Rather, the community will likely need to agree upon an accepted convention [14].
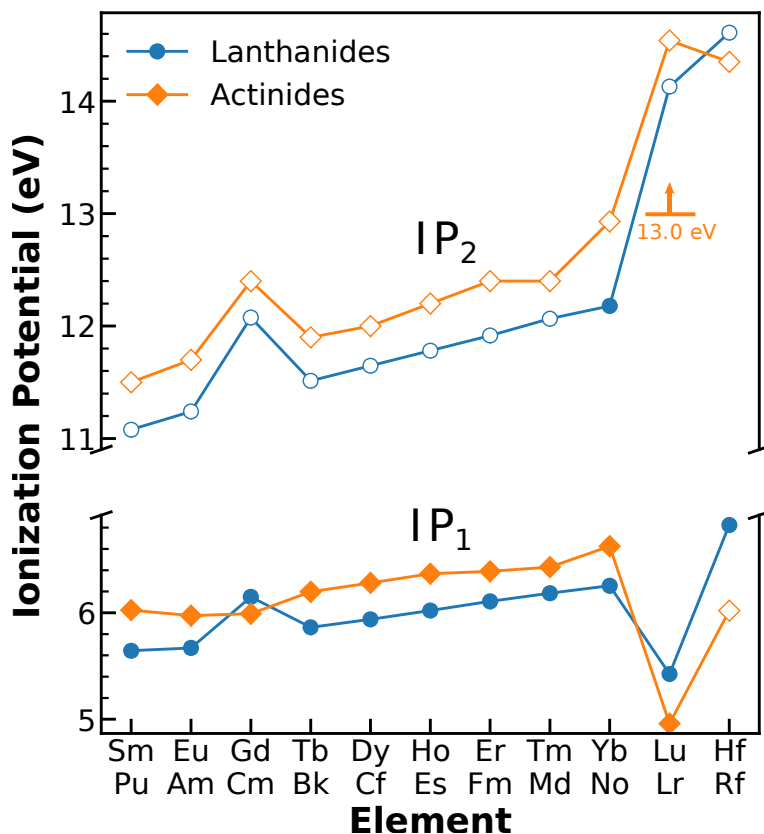

Figure 1 (color online): Trends in the first and second ionization potentials of the actinides (orange) and lanthanides plus Hf (blue) obtained from data in Ref. [27], except for the IP_1 of Fm and Md which are taken from Ref. [16]. The solid symbols represent experimentally determined values. Unfilled symbols represent values determined by interpolation or extrapolation of known experimental values or by semiempirical calculation, except for the IP_1 of Rf which is from theory, as are the IP_2 for Hf, No, Lr, and Rf. The error in the reported values are smaller than the plot symbols except for the IP_2 of the actinides for which the mean absolute deviations are 0.4 eV exclusive of Lr, and the error in the Fm and Md IP_1 determinations are both +/- 0.13 eV. The

bar and error represent the lower bound of the IP_2, fully including the experimental uncertainty, of Lr determined as the result of this work.

There are recent theoretical and experimental studies that have provided critical information to evaluate the placement of Lu and Lr [15-26]. Of these studies, perhaps the most compelling are those that can elucidate information on the first- (IP_1) and second-ionization potentials (IP_2) of these and neighboring elements. Comparisons of these values highlight the ionization potential trends in the region and provide insight on the electronic structure of these elements. The IP_1 and IP_2 values for the actinides and lanthanides are presented in Fig.1 as taken from Ref. [27]. The data presented in Fig. 1 show clear trends across the mid- to late late-actinide and lanthanide elements. The observed IP_1 values increase in energy from Tb and Bk until they drop suddenly for Lu and Lr, and the IP_2 values increase in energy from Tb and Bk before they increase dramatically for Lu and Lr. Both of these trends point towards the end of the lanthanide and actinide series with Lu and Lr, respectively. However, experimental measurements of the IP_2 values are necessary to validate these state-of-the-art theoretical calculations that take into account relativistic effects.

The desire to measure these IP_2 values is presently driving experimental advancement. Unfortunately, studies of elements with $Z \geq 100$ are extremely difficult. These elements do not exist naturally on earth and need to be produced one-atom-at-a-time in nuclear reactions. Isotopes of these elements are produced using nuclear fusion-evaporation reactions. In a fusion-evaporation reaction, a beam of an incident isotope impinges upon a target composed of heavy isotopes. The complete fusion of these two isotopes creates a compound nucleus that contains all of the protons and neutrons from the beam and target isotopes. Once created, these compound nuclei tend to be left in an excited state. One way they can de-excite is to evaporate off neutrons, leaving a final Evaporation Residue (EVR) that can be studied.

A new method for directly measuring the chemical properties of heavy and super heavy elements has been developed at the Lawrence Berkeley National Laboratory (LBNL) 88-Inch Cyclotron facility. This novel technique studies the chemical properties of these elements in the gas phase utilizing the combined capabilities of the Berkeley Gas-filled Separator (BGS) [28] and the recently-installed FIONA (For the Identification of Nuclide *A*) mass analyzer [29-31]. This setup allows for: (i) the production of ions of heavy and super heavy elements, (ii) separation of those ions from the beam and unwanted nuclear reaction products in the BGS, (iii) the ability to trap and cool the ions in an ion-trap in FIONA where (iv) reactive gas can be introduced and allowed to react with the trapped ions for a fixed interval of time, and (v) the number and mass of unreacted and reacted ions ejected from the trap can be directly measured. The new method is based off studies with Penning traps [32], inductively coupled plasma selected-ion flow tube (ICP/SIFT) [33], and Fourier transform ion cyclotron resonance mass spectrometry (FTICR-MS) [34]. Experimental studies using this technique can provide quantitative information such as ionization potentials, bond-dissociation energies, and kinematic reaction rates. Additionally, it is possible to directly confirm the production of various molecules from direct-mass number identifications.

This work reports the first experimental assessment of the IP_2 of Lr from the observation of the charge-transfer reaction between Lr^{2+} and O_2 gas. Not only can this result help to validate relativistic calculations, but it can also be used to better interpret the situation concerning the placement of Lu and Lr on the Periodic Table. This is the first-such experimental assessment of the IP_2 of any very-heavy actinide element. The success of this experimental technique has considerable implications as to the types of future measurements that can be performed on actinide elements. Additionally, there is clear feasibility demonstrated for similar studies of SHEs. Measurements performed with FIONA can be utilized not only to validate theoretical calculations, but to provide unprecedented knowledge on the properties of the heavy actinides and SHEs. This information can be used to better illuminate the proper organization of the Periodic Table.
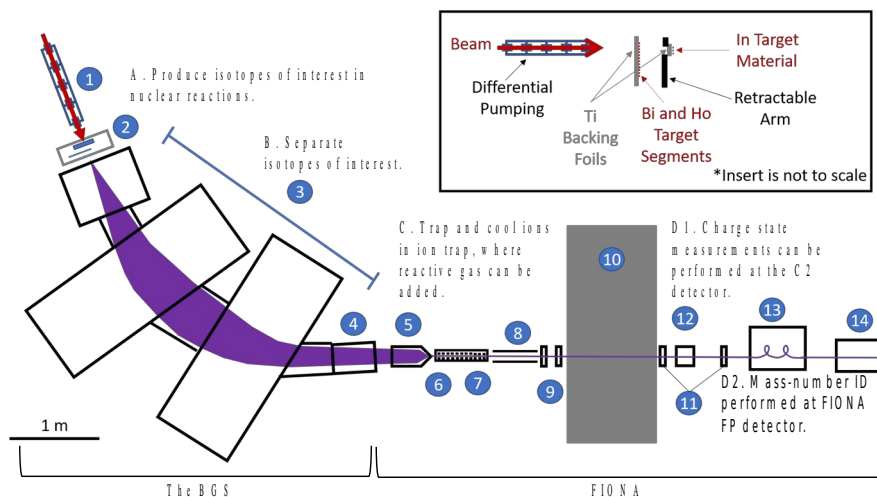
2. Experimental Methods

Figure 2 (color online): Schematic of the BGS and FIONA experimental setup. The labels indicate the positions of (1) the differential-pumping section, (2) the target chamber, (3) the BGS, (4) the BGS focal plane detector, (5) the RF Gas catcher, (6) the RFQ, (7) the RFQ trap, (8) the acceleration region, (9) a focusing element, horizontal and vertical steerers, (10) a shielding wall, (11) a focusing element, horizontal and vertical steerers, (12) the C2 detector, (13) the trochoid spectrometer, and (14) the FIONA FP detector. The purple shaded area/line represents the beam image of ions traveling through the BGS and FIONA. Additionally, the steps of a gas-phase chemistry experiment to be performed with this setup are indicated near the relevant sections of the setup. Note that only one of these measurements can be performed at a given time D1 or D2.

2.1 Nuclear Reactions

This experiment was performed at the LBNL 88-Inch Cyclotron facility. Ions of Lr were produced in the $^{209}Bi(^{48}Ca,2n)^{255}Lr$ nuclear reaction. In order to calibrate the system, ions of ^{151}Ho, $^{199-200}At$, and ^{208}Fr were produced in the $^{115}In(^{40}Ar,4n)$, $^{165}Ho(^{40}Ar,5\text{-}6n)$, and $^{165}Ho(^{48}Ca, 5n)$ reactions, respectively. The nuclear reactions discussed in this work along with the alpha energies of the produced isotopes are listed in Table 1.

Table 1: A list of the nuclear reactions discussed in this work. The detected alpha energies of the produced isotopes and the magnetic rigidity used to separate each respective isotope are also listed. Note that ^{216}Po is not produced from a nuclear reaction, but rather from an emanation source that is injected directly into the RF Gas Catcher.

4

Nuclear Reaction	Energy Range of Produced Isotopes (MeV)	magnetic rigidity (Tm)
^{209}Bi(^{48}Ca,2n)^{255}Lr	8.2 – 8.6	2.12
^{115}In(^{40}Ar,4n)^{151}Ho	4.2 - 4.6	1.67
^{165}Ho(^{40}Ar,5-6n) $^{199-200}$At	6.3 – 6.7	1.40
^{165}Ho(^{48}Ca, 5n)^{208}Fr	6.5 – 6.7	1.66
^{216}Po from ^{232}U emanation source	6.3 – 6.9	n/a – injected directly into RF Gas Catcher

Beams of ^{48}Ca^{11+} and ^{40}Ar^{9+} were sequentially produced from enriched-metallic Ca in VENUS (Versatile ECR ion source for NUclear Science) [35] or from natural Ar gas in the AECR (Advanced Electron Cyclotron Resonance ion source) [36]. The ions were then accelerated through the 88-Inch Cyclotron at LBNL to laboratory-frame energies of 232 MeV for ^{48}Ca and 200 MeV for ^{40}Ar with average intensities of 6 x10^{12} ion/s. A layout of the complete experimental apparatus is shown in Fig. 2. Each beam passed through a differential pumping section that separates the vacuum of the beamline from the 53 Pa He fill gas inside the BGS (Fig. 2, position 1). Immediately downstream of the differential pumping section, each beam impinged on a rotating (~30 Hz) target wheel (radius = 5.1 cm) consisting of four arc-shaped target segments (Fig. 2, position 2). Three of the segments were ^{209}Bi with an average thickness of 500(25) µg/cm^2, and the fourth target segment consisted of ^{165}Ho with an average thickness of 365(40) µg/cm^2. All target segments were prepared via vapor deposition on 2.1-µm thick Ti foil. It is expected that roughly 10 MeV of energy is lost through the Ti foil. Immediately downstream of the target wheel was an In target on an insertable arm. The In target was free-standing and composed of 1.5 mg of indium(III)nitrate hydrate deposited onto a 2.1-µm Ti foil. The In target had an approximate thickness of 1.5 mg/cm^2 and was inserted into the beam line via a target ladder (Fig. 2, position 2). The target was rectangular in shape with a circular active area one inch in diameter. Two passivated implanted planar silicon detectors, located at ±27.2° relative to the beam axis, were employed to count Rutherford scattered beam particles. This allowed for a continuous monitor of the integrated beam intensity and target thickness, as well as a check of the continued target integrity.

2.2 Isotope Separation with the BGS and FIONA

The compound nucleus EVRs produced in the ^{209}Bi(^{48}Ca,2n)^{255}Lr, ^{115}In(^{40}Ar,4n)^{151}Ho, and ^{165}Ho(^{40}Ar,5-6n)$^{199-200}$At reactions recoiled out of the target with the momentum of the beam and into the BGS. There, they were separated from the unreacted beam particles and unwanted reaction products based on their differing magnetic rigidities in 53 Pa He.

At the BGS focal plane, the EVRs passed through a 2.1-um thick Ti foil to enter the FIONA mass analyzer. Detailed descriptions of FIONA are given in Refs. [30, 31]. As a general description, FIONA was designed to stop and trap EVRs selected by the BGS and then transport them to a low- gamma and neutron radiation area for a mass-number identification. Within FIONA, the EVRs were initially stopped in 13 kPa of ultra-pure He (99.999%) inside of a radiofrequency (RF) Gas Catcher, where a fraction of the EVRs retained a positive charge. The

EVR ions are then pulled through the RF Gas Catcher using DC fields and the flow of the He gas. These ions then enter a two-stage radiofrequency quadrupole (RFQ), labelled as positions 6 and 7 in Fig. 2. Here, the ions are radially confined in the first stage (Fig. 2, position 6) of the RFQ while the He buffer gas is differentially pumped down to a pressure of ~30 Pa. Additionally, there is an axial DC gradient applied along the RFQ axis that then directs the ions to be captured in the second stage of the RFQ, a RFQ trap (Fig. 2, position 7). An axial DC gradient profile creates a 3-dimensional ion trap that confines ions to within a few mm^3. Continued-differential pumping on the RFQ trap maintains a He pressure of ~2 Pa, where collisions of the ions with the He buffer cool the ions to several times thermal energies. The ions are then ejected from the RFQ trap after a desired trapping interval. Trapping times can be selected ranging from 10 ms to 10 s. During this time ions are accumulated within the RFQ trap and contained by a positive potential well. They are then ejected from the potential well and extracted into the acceleration region. The acceleration region contains a pulsed drift tube. Once the ion bunch reaches the center of the drift tube, the potential is then inverted so that the ions are accelerated into the low-background area. There they are separated by their mass-to-charge-state ratio (A/q) before their trajectories terminate into a double-sided silicon detector (DSSD) for detection.

There are three identical 32 x 32 strip (2 mm/strip) DSSDs with active areas of 65 mm x 65 mm installed along the FIONA beamline. These three detectors will henceforth be referred to as the BGS Focal Plane (BGS FP), Cave 2 (C2), and FIONA Focal Plane (FP) detectors. Their positions are labelled as positions 4, 12, and 14 in Fig. 2, respectively. In each detector, the positions of events are given by the horizontal and vertical strip numbers in which each event was detected. Energies of alpha events detected in all detectors are calibrated using the alpha particles emitted from a source containing ^{239}Pu, ^{241}Am, and ^{244}Cm. A typical energy resolution for events detected during this experiment is on the order of 100-keV FWHM. The data acquisition was triggered by an alpha energy event in any of the detectors, greater than approximately 1 MeV. A typical transportation efficiency from the BGS focal plane through FIONA for detection at the FIONA focal plane is about 15%. This efficiency has been determined from the observation of EVR-alpha events observed at the BGS FP detector, as compared to events observed at the FIONA FP detector and is not element or species dependent.

FIONA separates ions by their A/q with the use of a trochoidal spectrometer [37]. The trochoidal spectrometer consists of crossed magnetic and electric fields, which force ions to follow trochoidal trajectories through the spectrometer [38-41]. The period and beam-direction precession of these trochoids is dependent on the A/q of a given ion and is largely independent of the ion velocity. The A/q separation occurs due to the difference in trochoid-phase for ions with different A/q. As ions of differing A/q exit the magnetic and electric fields of the spectrometer, the exit angles of their trajectories will differ. Given this, ions of different A/q will be detected in different areas of the FIONA focal plane DSSD. Therefore, the position of detection for these ions yields information as to their A/q. The mass resolving power of FIONA, with separation of masses at the full-width-at-tenth-maximum level is $(A/q)/\Delta (A/q) = 250$. A typical A/q dispersion for detected ions is ~18mm/1%$\Delta (A/q)$. For example, if neighboring isotopes of ^{255}Lr^{2+} and ^{256}Lr^{2+} ions were both to be produced in the nuclear fusion-evaporation reaction, both being delivered to the FIONA focal plane, they are ~0.4% different in A/q. They would be separated by

~7 mm when they arrive for detection at the FIONA focal plane. As the DSSD detector is composed of 2-mm strips, a 7-mm separation allows for neighboring isotopes of the same element to be readily identified as they will be detected in different strips. In this measurement, a majority of the ions produced were [255]Lr. At most ~15% of the ions could be attributed to the production of [256]Lr.

The production isotopes of interest, and their transmission to each potential detection location, was confirmed using alpha spectroscopy. The [255]Lr, [151]Ho, [199-200]At, and [208]Fr isotopes all have different alpha-decay signatures that can be readily identified with the BGS FP, C2, and FP detectors. Note that the BGS separates ions based on their magnetic rigidity in He gas and has an acceptance of ~±3% Brho. Given that the magnetic rigidity of Lr, At, Fr and Ho are approximately 2.12 Tm, 1.67 Tm, 1.66 Tm, and 1.40 Tm, respectively, and that At and Fr were not made simultaneously, only one element was transmitted to the detectors at a time. Details of the BGS and the separation procedures can be found in [28].

The BGS FP detector can be inserted into the beamline at the BGS focal plane (Fig. 2, position 4) to observe the alpha-decay energies of any implanted EVRs selected for transmission by the BGS. The BGS FP detector is also used to see if the EVRs are centered as they exit the BGS, such that good transmission can be achieved in entering FIONA. When the BGS FP detector is retracted, the produced EVRs pass through a 2-um thick titanium window and in FIONA. The C2 detector (Fig. 2, position 12) can be inserted into the beamline to observe the alpha-decay energies and spatial distribution of the EVR ions once they have been re-accelerated into the low-background area from the RFQ trap. The FIONA FP detector (Fig. 2, position 14) is located ~75 cm downstream from the exit of the trochoidal spectrometer. At the FIONA FP detector, the position of detected events is used for mass-number identification of the produced EVR ions. Note that at the C2 and FP detectors there is no implant signal detected for the EVRs, only their alpha decays are observed. Additionally, events detected with the FIONA FP detector are separated and can be identified by their A/q, whereas events detected with the BGS FP and C2 detectors are not.

2.3 Gas Phase Ion Chemistry with FIONA

It is possible to perform gas-phase chemistry investigations with the FIONA apparatus by adding reactive gas to the RFQ trap (Fig. 2, position 8). In these studies, the ions of interest are produced as described previously, and are then accumulated and trapped in the RFQ trap for a fixed-time interval with a select concentration of reactive gas. The reactive gas is injected directly into the RFQ trap with a controlled flow rate. During this trapping time, it is possible that ions undergo chemical reactions with the injected reactive gas. Note that in some instances, only a single ion will have accumulated within the trap during the chosen accumulation/trapping time. After the trapping time, all of the ions are ejected from the RFQ trap and reaccelerated into the low-background counting area. There, reaction products can be studied with either the C2 or FIONA FP detector.

The A/q of the produced ion or molecule can be directly determined by detection at the FIONA FP detector (Fig 2, position 14). For this measurement, once the A/q of reaction products had been identified, further measurements to study the chemical reaction were performed at the C2 DSSD detector (Fig. 2, position 12). It was advantageous to make measurements at the C2 detector as there is increased ion-transportation efficiency to that detector as compared to the downstream FIONA FP detector. This loss-mechanism from the C2 detector to the FIONA FP is independent of the A/q of the produced species.

Even though events cannot be directly identified at the C2 detector by their A/q, measurements there are charge-state selective. This is because the C2 detector is located downstream of a pulsed drift tube (Fig. 2, position 8). The pulsed drift tube operates by first electrostatically accelerating ions into the tube. Then, while ions are within the drift tube, there is a pulsed reversal in the electrical polarity such that the ions are accelerated as they exit the tube. The time interval between ejecting the ions from the RFQ trap and pulsing the drift tube establishes a charge state-sensitive "drift time". Different charge states are accelerated to different velocities. This means that different charge states of the same element require distinct drift times for re-acceleration to successfully traverse the drift tube. This allows for the ability to selectively re-accelerate a single charge state by properly choosing the appropriate drift time. An example is shown in Fig. 3 for ^{208}Fr ions. Here, the 1+ and 2+ ions were found to be best accelerated with drift times of 27.5 and 19 μs, respectively.
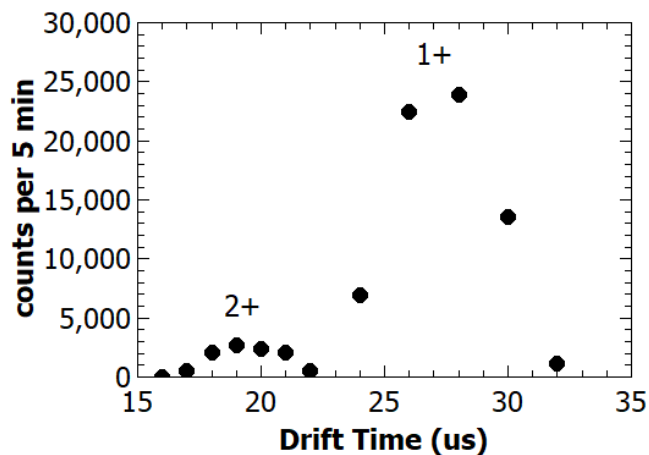

Figure 3: The number of counts of ^{208}Fr observed on the C2 detector as a function of the drift time through the pulsed drift tube.

This novel approach and technique, utilizing FIONA, can be used to perform gas-phase chemistry studies with ion generation rates as low as one atom-at-a-time. Meaning that single ions can be produced and then trapped for chemical studies. This extreme sensitivity allows for unprecedented measurements that can determine fundamental chemical properties of elements with $Z \geq 100$ not typically available for studies in a traditional radiochemical-laboratory environment. Most notably, this includes potential studies of SHEs. Of initial interest, and importance, are studies of charge-exchange reactions. These measurements can bracket the upper and lower limits of heavy ion IPs. The determination of these limits depends intimately on what

class of reaction can take place and whether a reaction can or cannot occur with a particular reactive gas species. Thus, the selection of a proper reactive gas is critical and can effectively establish one of the two IP limits, either upper or lower. This bracketing technique has already been shown to be successful in bracketing IPs to within 0.1 eV with radioactive ions that are readily accessible within a more-standard radiochemical-laboratory environment [42]. Additionally, the ability to control the reaction times and the concentration of reactive gas within the RFQ trap allows for the determination of chemical reaction rates. Furthermore, the production of any molecular ions can be directly confirmed with mass number identifications performed with the FIONA mass analyzer. These measurements are of critical importance towards understanding the chemical properties of the heaviest elements.

3. RESULTS AND DISCUSSION

3.1 Pressure Calibrations and Gas Composition for the RFQ trap

In this work, all chemical reactions were performed with O_2 gas. An estimate of the partial pressure of the O_2 gas in the RFQ trap is given by a residual gas analyzer (RGA). As the RGA is positioned downstream of the RFQ trap and connected by approximately two meters of vacuum line, it does not read the true pressure inside of the RFQ trap. In order to determine the true partial pressure of O_2 in the RFQ trap, a simple calibration was performed. The reaction

$$Ho^{+} + O_2 \rightarrow HoO^{+} + O \qquad (1)$$

has been studied previously and has a well-known pseudo-first order reaction-rate constant $k = 2.4(7) \times 10^{-10}$ cm^3/molecules/s [43]. This reaction was performed so that a calibration factor (f) could be determined to scale $[O_2]_{RGA}$ to that of the true concentration of O_2 in the RFQ trap ($[O_2]_{true}$), where $[O_2]_{true} = f [O_2]_{RGA}$.

The Ho$^+$ ions were produced in the nuclear reaction ^{115}In(^{40}Ar,4n) ^{151}Ho. Controlled flow rates of O_2 gas were added to the RFQ trap and the number of ^{151}Ho$^+$ and ^{151}HoO$^+$ ions produced were measured at the FIONA FP detector. Ions were directly identified as either $A/q = 151/1$ or $A/q = 167/1$, indicating the detection of ^{151}Ho$^+$ and ^{151}HoO$^+$ ions, respectively. From these measurements, f was determined to be $3.2(12) \times 10^{19}$ molecules/cm^3. The establishment of f made it possible to perform other chemical reactions with O_2 gas as $[O_2]_{true}$ could be readily determined. Further details of these measurements are provided in the Supporting Information.

The general composition of the gas within the RFQ trap was monitored with the RGA. The RGA readings of each observed gas are listed in Table 2. Note that readings from the RGA cannot be used to determine the exact fraction of various gasses in the RFQ Trap, as the RGA is more sensitive to gasses with lower ionization potentials. However, It is clear O_2 is the dominant species observed within the RFQ trap, except for the added He buffer gas.

Table 2: Gases identified with the RFQ trap with the RGA. Observed readings are shown relative to that of the added O_2 gas.

Identified Gas	RGA reading
H_2	0.23
He	3060

H_2O	1.40
N_2	3.01
O_2	100
Ar	0.21
CO_2	0.39

3.2 Production of ^{255}Lr Ions

The production of ^{255}Lr ions from the ^{48}Ca+^{209}Bi reaction was confirmed with the observation of signature alpha decays on the BGS FP detector. Alpha events with energies between 8.2 and 8.6 MeV were assigned as originating from the decay of ^{255}Lr. These events are shown in Fig. 4(a). Transmission of ^{255}Lr to the C2 and FP detectors was also confirmed with the observation of these same ^{255}Lr alpha decays. Figures 4(b) and 4(c) show the detected alpha energies for ^{255}Lr at the C2 and FP detectors, respectively. A rate of approximately 0.07 Hz was observed for ^{255}Lr ions detected at the C2 detector. Considering the transmission and detection efficiencies of transporting the ions to the C2 detector from their initial recoil out of the target upstream of the BGS, this corresponds to a production cross-section on the order of roughly 200 nb. This is in line with the observed cross section of ^{255}Lr reported previously for this reaction [44]. Note that the cross section of ^{255}Lr was not determined from data collected at the BGS focal plane due to the high-rate of background events observed at that location.
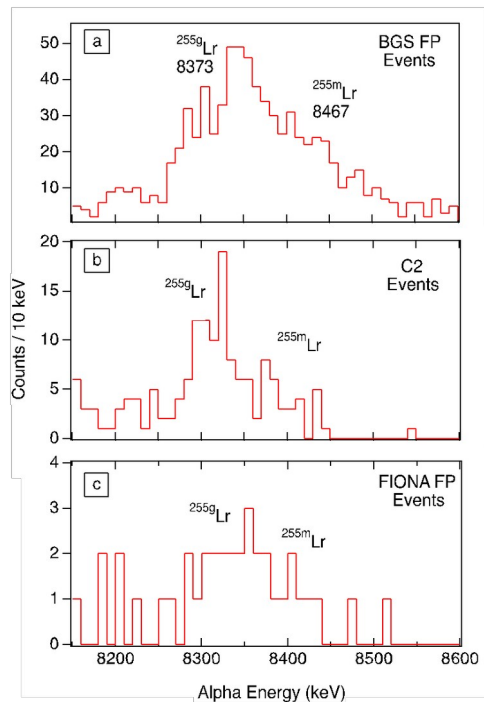

Figure 4 (color online): Energies of ^{255}Lr events detected at the (a) BGS FP, (b) C2, and (c) FIONA FP detectors.

3.3 Baseline ^{255}Lr Charge State Distributions in FIONA

Produced EVRs of elements of interest are partially stripped of electrons as they pass through the Ti window separating the BGS and FIONA. As these ions are stopped in the FIONA RF Gas

Catcher (Fig. 2, position 5), they exchange electrons with the He buffer gas and any contaminants in the system and will stop with a distribution of charge states. For a given element, this distribution of charge states is dependent on the IP_1, IP_2 and third-ionization potentials (IP_3) of the stopped element as compared to the IP_1 of the gases present in the FIONA system. Prior to performing any chemical reaction, it was necessary to determine the dominant charge states of the Lr ions as they traversed the FIONA apparatus. Note that these were baseline measurements before O_2 gas was introduced to the RFQ trap.

The charge state distribution of ^{255}Lr ions stopped in the FIONA system was measured at the C2 detector. As was discussed in section 2.3, measurements at the C2 detector are sensitive to differences in charge state. Ions of ^{255}Lr^{1+} and ^{255}Lr^{2+} were observed at the C2 detector with drift times of 28 μs and 20 μs, respectively. In both instances the selected RFQ trapping time was 100 ms.. From these measurements, 7(1)% of the ^{255}Lr ions were identified as ^{255}Lr^{1+} and 93(1)% of the ions were identified as ^{255}Lr^{2+}.

3.4 The Reduction of ^{255}Lr^{2+} to ^{255}Lr^{1+}

The baseline charge-state distribution measurements revealed the dominant ion to be ^{255}Lr^{2+} without any additional gases added to the FIONA apparatus. The reduction reaction

$$255\,Lr^{2+¿} + O_2 \rightarrow 255\,Lr^{1+¿ + O_{2:3}^{1+¿¿}}¿ \quad (2)$$
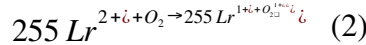
was then investigated. Measurements were performed at the C2 detector with drift tube pulse times of 20 μs and 28 μs for the detection of 1+ and 2+ ions, respectively. Initial measurements indicated that an increased production of the 1+ species was detected with the addition of O_2 gas flowing into the system. This increase in 1+ species could be due to the formation of ions of ^{255}Lr^{1+}, ^{255}LrO^{1+}, ^{255}LrOH^{1+}, etc. or some combination thereof. As there is no mass-selectivity for measurements at the C2 detector, the identity of the produced 1+ species needed to be directly confirmed with an A/q measurement at the FIONA FP detector.
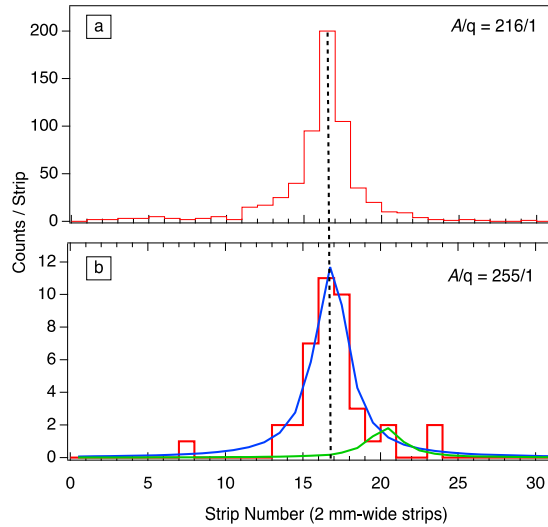

Figure 5 (color online): Distribution of events detected at the FIONA focal plane. In this instance, the electric fields of FIONA were scaled such that events of $A/q = 255/1$ would be detected in the same position as events with $A/q = 216/1$. (a) Detection position of the $A/q = 216/1$ ^{216}Po^{1+} ions. These events were detected primarily in x-strips 15-17 with the centroid fitted to be

16.02(4). (b) Detection position for $A/q = 255/1$ ions. Events were detected primarily in x-strips 15-17 with the centroid fitted to be 16.21(6). The Lorentzian fits are shown for $A/q = 255/1$ (blue) and $A/q = 256/1$ (green). At most, 15% of these ions can be attributed to the production of ions with $A/q = 256/1$. As the $A/q = 255/1$ ions were detected in the same position as the $A/q = 216/1$ ions, $A/q = 255/1$ is confirmed for these lawrencium ions.

In order to perform a mass number measurement, FIONA is first calibrated with ions of an established A/q. This entails tuning FIONA, such that the calibration ions are delivered to the FIONA FP detector with high-transportation efficiency and good-mass resolution. Then the system can be scaled such that the mass number of ions with an unknown or disputed mass number can be determined. This technique is discussed in detail in Ref. [30]. In this instance, the employed calibration ions used were $^{216}Po^{1+}$. These ions originated from a ^{232}U source that emanated ^{220}Rn. To introduce these ions to the FIONA beam line, He gas is flowed over the source and then injected into the RF Gas Catcher (Fig. 2, label 3). For selection of ^{216}Po events, energy windows were chosen to be 6.3 – 6.9 MeV. As is shown in Fig. 5a, FIONA was tuned such that the $A/q = 216/1$ $^{216}Po^{1+}$ ions were detected primarily in x-strips 15-17 with the centroid fitted to be 16.02(4).

Measurements were then taken at the FIONA focal plane to identify the A/q of the produced 1+ species following the introduction of O_2 gas to the RFQ trap. FIONA was scaled to transport ions with $A/q = 255/1$ for the delivery of $^{255}Lr^{1+}$ ions to the FIONA focal plane. These measurements were performed with an O_2 flow rate of 1.2×10^{-4} mbar L s^{-1} with a 100 ms trapping time. To be considered as potential ^{255}Lr events, observed alpha decays had to be in the energy range of 8.0 – 8.7 MeV. Statistics were collected for 3 hours and 41 events were recorded. As is shown in Fig. 5b, these events were detected primarily in x-strips 15-17 with the centroid fitted to be 16.21(6). As these ions were detected in the same position as the $A/q = 216/1$ ions, an A/q identification of 255/1 was confirmed for the produced lawrencium ions. This is a direct observation that $^{255}Lr^{1+}$ ions were produced as a result of the charge exchange reaction of $^{255}Lr^{2+}$ ions with O_2 gas as shown in eqn. 2.

Possible other 1+ reaction products such as $^{255}LrO^{1+}$, $^{255}LrOH^{1+}$, etc. were also considered to have been produced, as previous measurements had observed the production of LuO^{1+} [33]. The electric fields of FIONA were scaled to look for masses in the range of ~268-275 with charge state 1+ and the production of a small amount of LrO^+ or $LrOH^+$ was observed, estimated to be ~10% of the 1+ products. Given this, it is expected that these other reaction pathways do not substantially detract from the results reported here for the primarily-observed charge exchange reaction. Future measurements could be done in the future to better quantify the production of these other reaction pathways.

Once the detected 1+ species was determined to be primarily composed of $^{255}Lr^{1+}$ ions, more detailed measurements were performed to study the reduction reaction. The composition of the 2+ species was assumed to be primarily $^{255}Lr^{2+}$, but the exact ion-species composition was not experimentally verified. Charge state distribution measurements were performed at the C2 detector to determine the relative population of the $^{255}Lr^{2+}$ and $^{255}Lr^{1+}$ ions with varying concentrations of O_2 gas present in the system. The results of these measurements are summarized in Table 3 and plotted in Figure 6. Controlled O_2 flow rates into the trap were varied from 6.0×10^{-6} to 6.0×10^{-4} mbar L s^{-1}. For each flow rate, two separate measurements were taken.

The first was to observe the number of produced $^{255}Lr^{1+}$ ions and the second, to observe the produced $^{255}Lr^{2+}$ ions. Then, the charge state distribution could be determined for each O_2 flow rate. In all measurements, the selected RFQ-trapping time (reaction time) was 100 ms and the O_2 pressure in the RFQ trap was determined from the calibration established in section 3.1. For each measurement, statistics were collected on the C2 detector for thirty minutes and results were normalized to the recorded Rutherford rates to account for fluctuations in the beam intensity.

Table 3: Summary of $^{255}Lr^{2+}$ to $^{255}Lr^{1+}$ reduction measurements with O_2 gas. Separate measurements were performed for the detection of the $^{255}Lr^{2+}$ to $^{255}Lr^{1+}$ ions. For each measurement, the O_2 flow rate (mbar L s^{-1}), $[O_2]_{RGA}$, the trap cycle time (t_{cyc}, ms), and the fraction of observed $^{255}Lr^{1+}$ to $^{255}Lr^{2+}$ ions is listed.

O_2 Flow Rate (mbar L s^{-1})	$[O_2]_{RGA}$	t_{cyc} (ms)	Fraction of $^{255}Lr^{1+}$	Fraction of $^{255}Lr^{2+}$
0	5.0(5)x10^{-11}	100	0.074(21)	0.926(21)
6.0x10^{-6}	5.2(5)x10^{-10}	100	0.211(44)	0.789(44)
4.0x10^{-5}	1.1(1)x10^{-9}	100	0.328(47)	0.672(47)
1.2x10^{-4}	2.1(2)x10^{-9}	100	0.405(48)	0.595(48)
6.0x10^{-4}	4.5(5)x10^{-9}	100	0.593(45)	0.407(45)

To determine the reaction rate constant k for this reduction reaction, the $^{255}Lr^{2+}$ data were fit with Eqn. S1. Note that as f was determined to be 3.2(12) x10^{-19} molecules/cm^3, f $[O_2]_{RGA}$ could be replaced with $[O_2]_{true}$. A reaction rate constant of k=1.5(7)x10^{-10} cm^3/molecules/s was determined for the charge exchange reaction between $^{255}Lr^{2+}$ and O_2. Then, given k, the $^{255}Lr^{2+}$ data was fit with Eqn. S3. The reaction probability, k/k_c, for the charge exchange reaction between $^{255}Lr^{2+}$ ions and O_2 was determined with the collision rate coefficients, k_c, calculated using the algorithm of the modified variational transition-state/classical trajectory theory from Su and Chesnavich [45] and was determined to be 0.27.
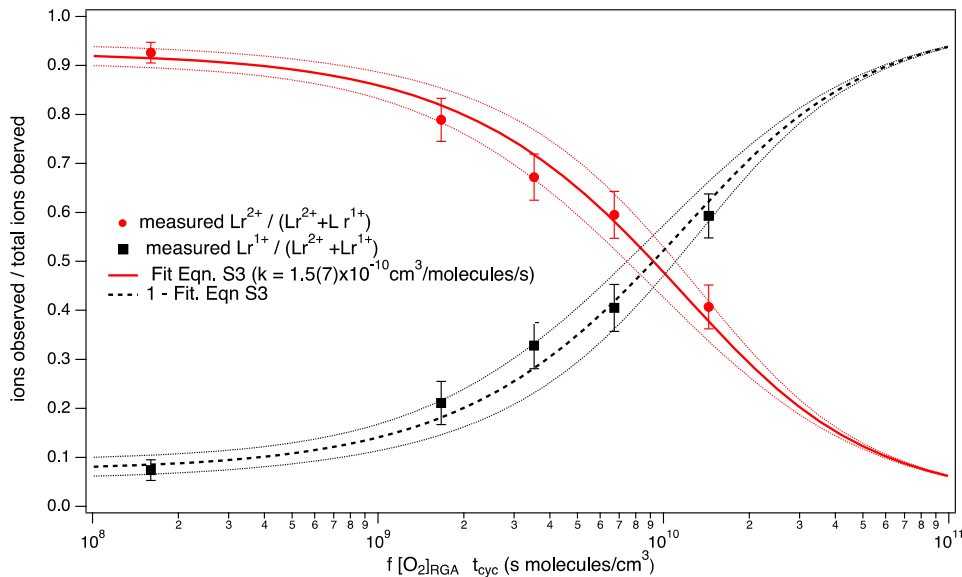
Figure 6 (color online): Fractions of $^{255}Lr^{2+}$ (red circles) and $^{255}Lr^+$ (black squares) plotted versus trap cycle time (t_{cyc}, ms) multiplied by [O_2] pressure recorded at the FIONA RGA on a logarithmic scale. All data were measured at a trapping time of 100 ms. The $^{255}Lr^{2+}$ data was fit with Eqn. S3, shown with the solid red line. The $^{255}Lr^+$ data is shown plotted against 1 - Fit. Eqn. S3 (black dashed line). Confidence intervals of 68% are shown for each fit.

3.5 Implications for the Second-Ionization Potential of Lawrencium

There have been previous experimental studies of the first-ionization potentials of the heavy actinide elements Fm ($Z=100$), Md ($Z=101$), No ($Z=102$), and Lr ($Z=103$) [15-17]. The first ionization potential of lawrencium was determined to be $4.96^{+0.05}_{-0.04}$eV [10], much lower in energy (~1.5 eV) than those of the other late-actinides. This measurement indicated that Lr had a loosely-bound electron in a valence orbital outside of closed shells. Theoretical predictions, taking into account relativistic effects, were able to successfully reproduce Lr's observed low IP_1. These suggested that the ground state electronic configuration for Lr is [Rn]$5f^{14}7s^27p$ [18-26]. These measurements of the IP_1 values for the late-actinide elements indicated that the 5f orbital is first fully-occupied at No, whose electron configuration is predicted to be [Rn]$5f^{14}7s^2$ [16]. This result confirms that the actinide series ends with Lr as had been predicted by Seaborg [9, 10].

Prior to this work, there were no previous experimental studies of the second-ionization potentials of these late-actinide elements. Theoretical predictions for the IP_2 of Yb, Lu, No, and Lr are listed in Table 4. It is expected that the IP_2 of Lr would be relatively large compared to its No, as removing two electrons would break into the closed-shell [Rn]$5f^{14}7s^2$ core. Confirmation of this large relative difference in IP_2 for these elements would further validate Lr as the end of the actinide series. Note that the same behavior is expected for the end of the lanthanide series, where the IP_2 of Lu is expected to be much higher than that of Yb. This is due to the prediction that removing two electrons from Lu would break into the closed-shell [Xe] $5f^{14}6s^2$ core.

In this work, we have shown that $^{255}Lr^{2+}$ ions can be reduced to $^{255}Lr^{1+}$ ions with the introduction of O_2 gas. The confirmation that this reduction reaction proceeds allows for the determination of the lower bound on the IP_2 of Lr. When a charge-exchange reaction takes place, the reactants must first overcome a Coulomb barrier. In previous studies of electron-transfer reactions between dipositive ions and neutral gas molecules, this barrier has been observed to be approximately 1.2(3)

Table 4: Theoretical and experimental values for the IP_2 of Yb ($Z=70$), Lu ($Z=71$), No ($Z=102$), and Lr ($Z=103$).

Reference	Approach	IP₂ Yb (eV)	IP₂ Lu (eV)	IP₂ No (eV)	IP₂ Lr (eV)
Pantazis & Neese [22]	DKH2-B3LYP[a]	-	-	12.99	14.53
Dzuba et al. (2014)[23]	CI+MBPT[b]	12.27	14.05	13.07	14.64
Dzuba et al. (2016)[24]	CI+all-order[c]	12.24	13.98	12.93	14.54
Liu et al.[25]	QRPP-CASSCF+AP	-	-	12.51	14.21

	CF[d]				
Cao et al.[26]	RPP-CASSCF+APCF[e]	-	-	12.52	14.22
	Measured	12.179185(25) [46]	-	-	>13.3(3) *this work*

[a] Second-order Douglas–Kroll–Hess approach combined with density functional theory (B3LYP functional)

[b] Relativistic configuration interaction (CI) combined with the linearized single–double coupled cluster method plus second-order many-body perturbation theory (MBPT).

[c] Relativistic configuration interaction (CI) combined with the linearized coupled cluster method plus all-order perturbation theory.

[d] Quasirelativistic ab initio pseudopotential (QRPP) complete active space self-consistent field (CASSCF) calculations combined with averaged coupled-pair functional (ACPF) and corrected for spin–orbit coupling

[e] Relativistic ab initio pseudopotential (RPP) CASSCF calculations combined with ACPF and corrected for spin–orbit coupling

eV [47]. Given this Coulomb barrier of 1.2(3) eV and that the well-known IP_1 of O_2 is 12.063(1) eV [48], it is possible to set a lower-limit on the IP_2 of lawrencium. The charge exchange between $^{255}Lr^{2+}$ ions and O_2 molecules would only occur if the IP_2 of Lr is greater than 13.3(3) eV, which establishes the lower limit for IP_2 of Lr as 13.0 eV. This lower limit is in accord with the predicted values for Lr listed in Table 4. In comparison to the predicted IP_2 values for No, this measurement establishes that removing two electrons from Lr requires breaking into closed-electron shell configurations. This gives further support to the Seaborg Actinide Hypothesis that the actinide series does end with Lr.

Future measurements need to be performed to more-precisely bracket the upper and lower-limits of IP_2 for Lr and No. For example, if Lr^{2+} were not observed to be reduced in a reaction with Ar gas (IP_1 = 15.759(1) eV [27]), then an upper-limit can be established on the IP_2 of Lr to be 14.6(3) eV. If the IP_2 of No were to be less than 13 eV, then a reduction of No^{2+} with O_2 should not be observed as it was here for Lr. A lower-limit of 10.5(3) eV could be set on the No IP_2 if the reduction of No^{2+} were observed to proceed with a reaction with NO gas (IP_1 = 9.2642(2) eV [27]). These measurements can be performed with FIONA in the future.

As for the discussion of the appropriate positioning of Lu and Lr on the Periodic Table, it is interesting to note that there is a previous study of the reduction of Lu^{2+} with O_2 gas [49]. In that study, it was observed that Lu^{2+} did not reduce to Lu^{1+} in the presence of the O_2 gas. Given the above discussion, this would indicate that the IP_2 of Lu is less than 13.3(3) eV. This is significantly lower than the present predictions listed in Table 4 for Lu. Given the analogous nature of Lu and Lr, this result could suggest that the IP_2 of Lr may also be closer to 13.3 eV as

opposed to the predicted Lr values above 14 eV. More experimental measurements need to be performed on both Lu and Lr to elucidate the matter.

4. CONCLUSIONS
The successful determination of the lower boundary of the Lr IP_2 and demonstration of gas-phase ion chemistry with FIONA is a major experimental advancement for studies of the chemical properties for elements that need to be created in nuclear reactions. Studies of these elements are needed to experimentally confirm the impact of relativistic effects in the region and to provide additional information on the arrangement of elements in the Periodic Table. Most importantly, this technique now creates the opportunity to perform studies with ion generation rates as low as one-atom-at-a-time, such that each individual measurement would be looking at the radioactive decay of a single atom. This creates the first opportunity for such measurements to be performed on SHEs. Future studies on the actinides and SHEs can extend beyond measuring reaction rates and bracketing ionization potentials to include confirming the formation of molecules with direct mass-number identifications. Such measurements would be critical aids towards the validation of theoretical predictions.

This is the first direct experimental assessment of the IP_2 for any transuranic element. From this work, the reduction of $^{255}Lr^{2+}$ ions with molecules of O_2 gas was successfully observed with the BGS-plus-FIONA setup at the LBNL 88-inch cyclotron. The reaction rate constant for the reaction was determined to be $1.5(7) \times 10^{-10}$ cm^3/mol/s. From this study, we report a lower limit on the IP_2 of Lr to be > 13.0 eV that establishes the Lr IP_2 is larger than the predicted IP_2 of No. This result not only lends general validation to the theoretical calculations for the IP_2 of Lr and the other actinides, it is in keeping with the periodic trends exhibited by or predicted for the lanthanide and actinide series as shown in Fig. 1. If the IP_2 of Lr had been observed to below 13 eV, or that of No, such a result would have raised immediate and further questions about the proper organization of the Periodic Table. The measured IP_1 [15,16] and IP_2 values for Lr confirm that it is the last actinide element, having a ground-state electronic configuration with a single weakly-bound electron outside a $[Rn]5f^{14}7s^2$ core. The 4.96-keV IP_1 is smaller than that measured for the other actinide elements, and the IP_2 > 13 eV is larger than that predicted for the other actinide elements. These data agree nicely with theoretical predictions, which suggest that the electronic orbitals in the first and second ionization are:

$$[Rn]5f^{14}7s^27p \rightarrow [Rn]5f^{14}7s^2 + e^- \text{ and } [Rn]5f^{14}7s^2 \rightarrow [Rn]5f^{14}7s + 2e^-,$$

respectively [18-26].

Future studies should be performed to more-precisely bracket the upper and lower limits on the IP_2 of Lr. In addition, we can expand these studies to other actinide elements to map out IP_2 trends in this region of the Periodic Table. This fundamental information, in conjunction with state of the art relativistic calculations, will unambiguously show that the Lu and Lr each contain one additional electron outside of fully-occupied f orbitals. This information can then be used by the community and the IUPAC working group to decide upon the composition of the group 3 elements and to further elucidate how the Periodic Table should be organized. The convention decided upon for group 3 would then fully resolve the debate on the Seaborg Actinide Hypothesis, either pointing to a finalized validation or necessary addendums.

ASSOCIATED CONTENT
Supporting Information
The Supporting Information is available free of charge at <mark>XXXXX</mark>

This information presented in the supporting information is to supplement the discussion of pressure calibrations in Section 3.1. The determination of the calibration factor f to scale the RGA pressure readings are given.

AUTHOR INFORMATION

Corresponding Author
Jennifer L. Pore – Nuclear Science Division, Lawrence Berkeley National Laboratory, Berkeley, CA, 94720, USA;
Email: JPore@lbl.gov

Authors
Jeffrey T. Kwarsick – University of California, Berkeley, Department of Chemistry, Berkeley, CA 94720, USA; Nuclear Science Division, Lawrence Berkeley National Laboratory, Berkeley, CA, 94720, USA;

Jacklyn M. Gates – Nuclear Science Division, Lawrence Berkeley National Laboratory, Berkeley, CA, 94720, USA;

Kenneth E. Gregorich – Nuclear Science Division, Lawrence Berkeley National Laboratory, Berkeley, CA, 94720, USA. Current Address: Lawrence Livermore National Laboratory, Livermore, CA, 94550;

John K. Gibson – Chemical Sciences Division, Lawrence Berkeley National Laboratory, Berkeley, CA, 94720, USA;

Jiwen Jian – Chemical Sciences Division, Lawrence Berkeley National Laboratory, Berkeley, CA, 94720, USA;

Gregory K. Pang – Nuclear Science Division, Lawrence Berkeley National Laboratory, Berkeley, CA, 94720, USA;

David K. Shuh – Chemical Sciences Division, Lawrence Berkeley National Laboratory, Berkeley, CA, 94720, USA; orcid.org/0000-0002-3104-3260

Notes

REFERENCES
1. Pershina, V. Electronic structure and properties of superheavy elements. *Nucl. Phys. A* **2015**, 944, 578-613.
2. Giuliani, S. A.; Matheson, Z.; Nazarewicz, W.; Olsen, E.; Reinhard, P. –G.; Sadhukhan, J.; Schuetrumpf, B.; Schunck, N.; Schwerdtfeger, P. Colloquium: Superheavy elements: Oganesson and beyond. *Rev. Modern Phys.* **2019**, 91, 011001.
3. Schädel, M. Chemistry of the Superheavy Elements. *Angew. Chem. Intl. Ed.* **2006**, 45, 368-401.
4. Schwerdtfeger, P.; Pašteka, L. F.; Punnett, A.; Bowman, P. O. Relativistic and quantum electrodynamic effects in superheavy elements. *Nucl. Phys. A* **2015,** 944, 551-577.
5. Türler, A.; Pershina, V. Advances in the Production and Chemistry of the Heaviest Elements. *Chem. Rev.* **2013**, 113, 1237-1312.
6. Chandrasekar, A.; Joshi, M.; Ghanty, T. K. On the position of La, Lu, Ac, and Lr in the periodic table: a perspective. *J. Chem. Sci.* **2019**, 131, 122.
7. Scerri E. Recent attempts to change the periodic table. *Phil. Trans. R. Soc. A* **2020,** 378, 2019300.
8. Vernon, R.E. The location and composition of Group 3 of the periodic table. *Found Chem* **2020**, 22.
9. Seaborg, G. T. The Chemical and Radioactive Properties of the Heavy Elements. *Chem. Eng. News* **1945**, *23*, 2190-2193.
10. Seaborg, G. T. The Transuranium Elements. *Science* **1946**, *104*, 379-386.
11. Seaborg, G.T. Origin of the Actinide Concept. *Handbook on the physics and chemistry of rare earths*, **1994**, 1-27.
12. Xu, W-H.; Pyykko, P. Is the chemistry of lawrencium peculiar? *Phys. Chem. Chem. Phys.*, **2016**,18, 17351-17355.
13. IUPAC Project: the constitution of group 3 of the periodic table, https://iupac.org/project/2015-039-2-200.
14. Scherri, E. Provisional Report on Discussions on Group 3 of the Periodic Table. *Chemistry International,* **2021,** 43(1), 31-34.

15. Sato, T. K.; Asai, M.; Borschevsky A.; Stora, T. Sato, N.; Kaneya, Y.; Tsukada, K.; Düllman, Ch. E.; Eberhardt, K.; Eliav, E.; et al. Measurement of the first ionization potential of lawrencium, element 103. *Nature* **2015,** 520, 209-211.

16. Sato, T.K.; Asai, M.; Borschevsky, A.; Beerwerth, B.; Kaneya, Y.; Makii, H.; Mitsukai, A.; Nagame, Y.; Osa, A.; Toyoshima, A.; et al. Verification of Filling-Up of 5f Electrons and Confirmation of the Actinide Series. *J. Am. Chem. Soc.* **2018**, 140, 44, 14609-14613.

17.   Chhetri, P.; Ackermann, D.; Backe, H.; Block, M.; Cheal, B.; Droese, C; Düllmann, Ch.E.; Even, J.; Ferrer, R.; Giacoppo, F. Precision Measurement of the First Ionization Potential of Nobelium. *Phys. Rev. Lett.* **2018**, 120, 263003.

18. Desclaux, J.-P.; Fricke, B. Relativistic prediction of the ground state of atomic lawrencium. *J. Phys.* **1980,** 41, 943–946.

19. Eliav, E.; Kaldor, U; Ishikawa, Y. Transition energies of ytterbium, lutetium, and lawrencium by the relativistic coupled-cluster method. *Phys. Rev. A* **1995**, 52, 291–296.

20. Zou, Y.; Fischer, C. F. Resonance transition energies and oscillator strengths in lutetium and lawrencium. *Phys. Rev. Lett*. **2002**, 88, 183001.

21. Borschevsky, A.; Eliav, E.; Vilkas, M. J.; Ishikawa, Y.; Kaldor, U. Transition energies of atomic lawrencium. *Eur. Phys. J. D* **2007,** 45, 115–119.

22. Pantazis, D.A.; Neese, F. All-Electron Scalar relativistic Basis Sets for the Actinides. *J. Chem. Theory Comput.* **2011,** 7 (3), 677-684.

23. Dzuba, V. A.; Safronova, M. S.; Safronova, U. I. Atomic properties of superheavy elements No, Lr, and Rf. *Phys. Rev. A* **2014**, 90, 012504.

24. Dzuba, V.A.; Safronova, U. I.; Safronova, M. S.; Kramida A. Ionization potentials of superheavy elements No, Lr, and Rf and their ions. *Phys. Rev. A* **2016**, 94, 042503.

25. Liu, W.; Kuchle, W.; Dolg. M. Ab initio pseudopotential and density-functional all-electron study of ionization and excitation energies of actinide atoms. *Phys. Rev. A* **1998,** 58(2), 1103.

26. Cao, X.; Dolg, M.; Stoll, H. Valence basis sets for relativistic energy-consistent small-core actinide pseudo potentials, *J. Chem. Phys* **2003**, 118, 487.

27. Kramida, A.; Ralchenko, Yu.; Reader, J.; NIST ASD Team (2019). *NIST Atomic Spectra Database* (ver. 5.7.1), [Online]. Available: https://physics.nist.gov/asd [2020, October 2]. National Institute of Standards and Technology, Gaithersburg, MD.

28. Gregorich, K. E. Simulation of recoil trajectories in gas-filled magnetic separators. *Nucl. Instrum. Methods A* **2013,** 711, 47-59.

29. Gates, J. M. Prospects of A and Z identification experiments at LBNL. *EPJ Web Conf.* **2016**, 131, 08003.

30. Gates, J. M.; Pang, G. K.; Pore, J. L.; Gregorich, K. E.; Kwarsick, J. T.; Savard, G.; Esker, N. E.; Kireef Covo, M.; Mogannam, M. J.; Batchelder, et al. First Direct Measurements of Superheavy-Element Mass Numbers, *Phys. Rev. Lett* **2018**, 121, 222501.

31. Gates, J. M.; Gregorich, K. E.; Pore, J. L.; Pang, G. K.; Kwarsick, J. T.; Kireef Covo, M.; Savard, G.; Esker, N. E. The FIONA mass analyzer for heavy element studies at LBNL, to be submitted 2021.

32. Rieth, U.; Herlet, A.; Volker Kratz, J.; Schweikhard, L.; Vogel, M.; Walther, C. *et al.* Ion-molecule reactions of Ru^+ and Os^+ with oxygen in a Penning trap. *Radiochim. Acta* **2002,** 90, 337.

33. Koyanagi, G. K.; Bohme, D. K. Oxidation Reactions of Lanthanide Cations with N2O and O2: Periodicities in Reactivity. *J. Phys. Chem. A* **2001**, 105, 8964-8968.

34. Santos, M.; Marçalo, J.; Leal, J. P.; Pires de Matos, A.; Gibson, J. K.; Haire, R. G. FTICR-MS study of the gas-phase thermochemistry of americium oxides. *Int. J. of Mass Spectrom.* **2003,** 228, 457-465.

35. Lyneis, C. M.; Leitner, D.; Leitner, M.; Taylor, C.; Abbot, S. The third generation superconducting 28 GHz electron cyclotron resonance ion source VENUS. *Rev. Sci. Instrum.* **2010**, 81, 02A201.

36. Xie, Z. Q. ; Lyneis, C. M. Performance of the upgraded LBNL AECR ion source. *LBNL-40155, UC-413* **1997**.

37. Mariner, T.; Bleakney, W. A Large Mass Spectrometer Employing Crossed Electric and Magnetic Fields. *Rev. Sci. Instrum.* **1949**, 20, 297.

38. Monk, G.W.; Werner, G. K. Trochotron Design Principles. *Rev. Sci. Instrum.* **1949**, 20, 93.

39. Robinson, C.F.; Hall, L. G. Small General Purpose Cycloidal-Focusing Mass Spectrometer. *Rev. Sci. Instrum.* **1956**, 27, 504.

40. Yano, K.; Be, S. H. Mass Analysis of Cluster Ion-Beams by Wien Filter. *Jpn. J. Appl. Phys.* **1980**, 19, 1019-1025.

41. Santos, M.; Marçalo, J.; Leal, J. P.; Pires de Matos, A.; Gibson, J. K.; Haire, R. G. Gas-Phase Ovidation Reactions of Neptunium and Plutonium Ions Investigated via Fourier Transform Ion Cyclotron Resonance Mass Spectrometry. *J. Phys. Chem. A* **2002**, 106, 7190.

42. Gibson, J. K.; Haire, R. G.; Marçalo, J.; Santos, M.; Pires de Matos A.; Leal, J.P. Determination of the ionization energy of NpO_2 and comparative ionization energies of actinide oxides. *J Nucl. Mater.* **2005**, 344, 24-29.

43. Koyanagi, K.; Bohme D. K. Oxidation Reactions of Lanthanide Cations with N_2O and O_2 Periodicities in Reactivity. *J. Chem. A* **2001**, 105, 39, 8964-8968.

44. Gaggeler, H. W.; Jost, D. T.; Turler, A.; Armbruster, P.; Bruchle, W., Folger, H.; Hebberger, F. P.; Hofmann, S.; Munzenberg, G.; Ninov, V. Cold Fusion Reactions with 48Ca. *Nucl. Phys. A* **1989**, 502, 561c.

45. Su, T.; Chesnavich, W. J. Parametrization of the ion–polar molecule collision rate constant by trajectory calculations. *J Chem. Phys.* **1992**, 76, 5183-5185.

46. Maeda, H.; Mizugai, Y.; Matsumoto, Y.; Suzuki, A.; and Takami, M.; Highly Excited Rydberg Series of Lu I Studied by Two-Step Laser Photoionisation Spectroscopy, *J. Phys. B* **1989**, 22, L511.

47. Gibson, J. K.; Haire, R. G.; Santos, M.; Marçalo, J.; Pires de Matos, A. Oxidation Studies of Dipositive Actinide Ions, An^{2+} (An = Th, U, Np, Pu, Am) in the Gas Phase: Synthesis and Characterization of the Isolated Uranyl, Neptunyl, and Plutonyl Ions UO22+(g), NpO_2^{2+}(g), and PuO_2^{2+}(g). *J Phys. Chem. A* **2005**, 109, 2768-2781.

48. Samson J. R. A.; Cains, R. B. Ionization Potential of O_2, *J. Opt. Soc. Am.* **1966**, 56(6), 769.

49. Gibson, J. K.; Haire, R. G.; Santos, M.; Pires de Matos A.; Marçalo, J. Gas-Phase Oxidation of Cm[+] and Cm[2+] -Thermodynamics of Neutral and Ionized CmO. *J Phys. Chem. A* **2008**, 112, 11373-11381.

Table of Contents Graphic